Acta Cryst. (1997). B53, 831–837

Structure Analysis of C_{60} Low-Temperature Phase by Electron Crystallography with Cryo-TEM

TETSUYA OGAWA,* SEIJI ISODA AND TAKASHI KOBAYASHI

Institute for Chemical Research, Kyoto University, Uji, Kyoto 611, Japan. E-mail: ogawa@eels.kuicr.kyoto-u.ac.jp

(Received 8 November 1996; accepted 10 April 1997)

Abstract

The crystal structure of C_{60} at liquid helium temperature was examined by the electron diffraction method using an imaging plate and cryo-TEM (transmission electron microscopy). The crystal of C_{60} was so thin that the electron scattering from this sample was able to be treated kinematically. However, the least-squares fitting among observed and kinematically calculated diffraction intensities resulted in an R factor of 0.23 for a structure model with only one major orientation. Similar large R factors are usually reported in the electron crystallography of thin crystals, in which a single perfect structure was assumed as a model structure. By considering structural disorders in the C_{60} crystal, however, the R factor could be reduced to 0.12, when a minor crystal in a different orientation and also the f.c.c. (face-centered cubic) component were introduced to the model in addition to the major orientation crystal. Disorder in the crystal might be as important a factor as the dynamical scattering effect to be considered in electron crystallography for analyzing structures of thin crystals.

1. Introduction

In recent years much attention has been given to ultra-thin organic films and their electric and optical properties. Since such ultra-thin films sometimes exhibit polymorphs and pseudomorphs, knowledge of the crystal structures as well as the molecular structures becomes important for understanding the mechanisms of such characteristic electric and optical features. A transmission electron microscope (TEM) is a useful tool for studying the crystal structure of such specimens and high-resolution imaging, electron diffraction and microscopic analytical methods have been developed in the past few years. High-resolution imaging can often be used to decide the molecular packing in a unit cell, but an atomic level resolution is not easily attainable for organic crystals owing to severe radiation damage. Consequently, electron diffraction is mainly used to determine the symmetry of unit cells and the lattice parameters used in structure analysis. However, the diffraction intensity has not been widely used to determine crystal structure as in X-ray or neutron diffraction techniques, because the theoretical treatment of the diffraction data is not as simple due to the existence of the dynamical scattering effect and the lack of quantitative response of the conventional recording medium used until recently. However, Dorset and coworkers (Dorset, 1991) demonstrated the possibility of crystal structure analysis by the electron diffraction technique using the direct phasing procedure, where the dynamical scattering effect was ignored and the scattering intensities were only treated kinematically. In their analysis, and the following other analyses, the coincidence of the observed and the kinematically calculated intensities were not satisfactory. The dynamical scattering effect is often considered to be a reason for the inaccuracy of analysis. Some techniques have been used to diminish the dynamical effect, for example, employment of a high-voltage electron microscope and/or using ultra-thin samples. Even under such optimized conditions, however, the kinematical treatment gives only 0.2–0.3 as the R factor, which is worse compared with the results of X-ray or neutron scattering methods (Dorset, 1995).

We have been experimenting with the crystal structure analysis of ultra-thin organic films by electron diffraction using an imaging plate [IP (Ogawa, Moriguchi, Isoda & Kobayashi, 1994*a*,*b*)], which is well known as a recording medium for electron intensities. An IP exhibits a wide dynamic range over four orders, a higher sensitivity of two orders than that of conventional electron microscopic films and a good linear response to electron dose. In addition, the digital output data are suitable for the quantitative treatment of diffraction intensity with a computer. These excellent properties make it possible to obtain precise electron diffraction intensities and to analyze crystal structure in atomic resolution, even when only one zonal pattern of electron diffraction can be obtained. In this report we analyze the crystal structure of C_{60} at liquid helium temperature using a 400 kV cryo-TEM and discuss the reason for the disagreement between the observed and the kinematically calculated intensities.

The C_{60} molecule forms a truncated icosahedron consisting of 12 pentagonal and 20 hexagonal faces (Kroto, Heath, O'Brien, Curl & Smalley, 1985). Although all atoms are identical (Johnson, Meijer & Bethune, 1990), there are two types of atomic bonds connecting them

ISSN 0108-7681

(Yannoni, Bernier, Bethune, Meijer & Salem, 1991). One is a shorter bond such as a double bond (*ca* 0.140 nm), which fuses two hexagons together and is often referred to as the 6:6 bond. The other is longer, such as a single bond (*ca* 0.145 nm), referred to as the 6:5 bond which fuses a hexagon and a pentagon in a molecule. The C_{60} crystal has a face-centered cubic (f.c.c.) lattice and at room temperature the soccer ball molecule rotates freely around its center. The crystal has a first-order rotational transition point around 260 K (Heiney *et al.*, 1991) and also an orientational glass transition around 86 K (David, Ibberson, Dennis, Hare & Prassides, 1992; Matsuo *et al.*, 1992). Below the first-order transition point, free rotation of the molecule is partly restricted and the crystal symmetry becomes $Pa\bar{3}$ of a simple cubic from $Fm\bar{3}$ of f.c.c. (Sachidanandam & Harris, 1991), although the center of molecule still lies on an f.c.c. lattice. Below the glass transition point, residual freedom of rotation is completely frozen. In this work we investigated the diffraction pattern of thin C_{60} crystals in this frozen state at liquid helium temperature to analyze the structure and revealed a disordered structure in thin crystals.

2. Methods and materials

The thin crystalline sample was prepared by vacuum deposition of C_{60} in a vacuum of 1×10^{-5} Pa onto a (001) cleavage surface of KI substrate at 433 K, which was preheated at 673 K for 1 h. The thickness of the deposited film was monitored by a quartz oscillating microbalance to be less than 10 nm. The deposition rate was controlled to be slower than 1 nm min^{-1}. After back-coating with a thin amorphous carbon film, the sample was stripped off by floating it on water and fixed on a micro-grid. The TEM used was JEM-4000SFX operated at the acceleration voltage 400 kV. This TEM is equipped with a cryo-stage cooled by liquid helium so that the sample is observed at the temperature 4.2 K. An electron diffraction pattern with the incident beam along <111> was observed and recorded on an IP. The high accelerating voltage is effective at reducing the dynamical scattering effect and also useful at reducing the specimen damage by electron irradiation, especially for organic materials. Moreover, we used cryo-stage and a high-sensitivity IP so that the damage of the specimen was almost negligible during the intensity data collection. The IP used was DL-UR_{III} of Fuji Film Co., where the active area size was 102×77 mm^2. The diffraction pattern recorded was read by a PIXsysTEM image reading system supplied by JEOL. The read-out area is 2048×1536 pixels and each pixel size is 50×50 μm^2. The output value as an intensity varies from 0 to 4095. The output value was transformed to electron dosage for each pixel using the calibration relationship reported previously (Isoda, Saitoh, Moriguchi & Kobayashi, 1991). The integral intensity of each diffraction spot was estimated by summing up intensity values in a circular region around a spot, after subtracting the background determined by the least-squares fit of its level in a doughnut region outside the circular region. Finally, the integral intensities were averaged over symmetrically equivalent reflections. These intensity data were compared with those calculated from model structures.

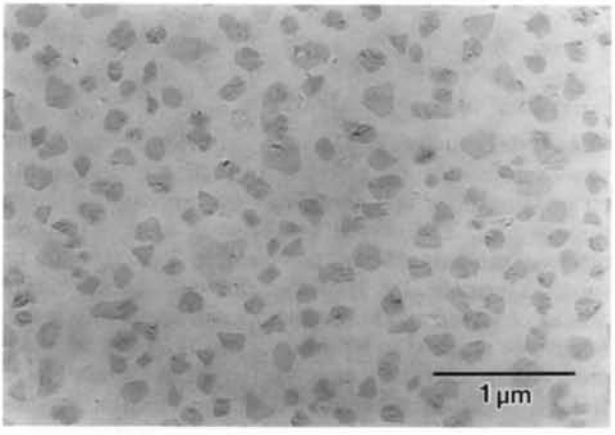

Fig. 1. Vacuum-deposited C_{60} crystals onto the KI substrate at 433 K. Almost all the crystals show truncated triangular or hexagonal shape and the {111} plane is parallel to the substrate surface. Some crystals show another orientation, that is, the {110} or {100} plane parallel to the substrate.

Fig. 2. Electron diffraction pattern of the C_{60} low-temperature phase with the incident beam parallel to the <111> direction. It shows sixfold rotational symmetry corresponding to the space group $Pa\bar{3}$. In the center of the triangles of intense spots near the center beam there are some weak spots arising from planar disorder, such as stacking faults on the (111) plane, which cause reciprocal lattice nodes of the upper zone such as the 111 reflection to be streaked (Ishiguro & Hirotsu, 1992).

Table 1. *Observed and calculated structure factors*

hkl	$\lvert F_{obs}\rvert$	$\lvert F_{calc}\rvert$ Case 1	Case 2	Case 3	*hkl*	$\lvert F_{obs}\rvert$	$\lvert F_{calc}\rvert$ Case 1	Case 2	Case 3
$2\bar{2}0$	100.00	92.02	—	96.24	$5\bar{8}3$	2.64	0.53	1.00	0.94
$1\bar{3}2$	2.35	1.99	1.49	1.56	$3\bar{8}5$	3.06	1.67	1.80	1.74
$2\bar{3}1$	4.44	2.87	2.06	2.14	$1\bar{8}7$	2.93	3.90	5.17	5.30
$2\bar{4}2$	40.80	39.28	—	41.29	$7\bar{8}1$	6.37	8.97	7.53	7.87
$1\bar{4}3$	4.84	5.55	3.84	4.20	$5\bar{9}4$	3.38	1.09	3.41	3.20
$3\bar{4}1$	4.75	6.17	4.37	4.81	$4\bar{9}5$	6.65	8.34	7.02	7.39
$4\bar{4}0$	9.07	5.79	—	10.78	$6\bar{9}3$	2.67	2.07	1.94	1.92
$2\bar{5}3$	8.92	14.91	9.81	10.81	$8\bar{8}0$	8.12	8.67	—	8.86
$3\bar{5}2$	4.89	3.87	4.61	4.88	$2\bar{9}7$	2.30	2.88	2.65	2.70
$1\bar{5}4$	4.05	3.42	5.14	4.48	$7\bar{9}2$	2.48	2.55	2.49	2.55
$4\bar{5}1$	8.17	7.44	8.10	7.75	$1\bar{9}8$	4.49	3.91	3.90	4.07
$3\bar{6}3$	9.65	12.24	8.76	9.54	$7\bar{10}3$	3.27	1.07	2.04	1.40
$2\bar{6}4$	7.94	1.89	—	8.12	$2\bar{10}8$	6.01	4.59	—	5.42
$4\bar{6}2$	8.06	0.33	—	8.12	$8\bar{10}2$	6.65	4.77	—	5.42
$5\bar{6}1$	10.52	12.29	10.51	10.51	$1\bar{10}9$	4.05	3.62	4.69	4.53
$1\bar{6}5$	4.28	4.48	6.05	5.24	$9\bar{10}1$	3.21	1.32	2.74	2.44
$6\bar{6}0$	6.25	5.61	—	7.58	$7\bar{11}4$	5.38	4.22	4.74	4.70
$3\bar{7}4$	9.30	11.24	9.13	9.62	$10\bar{10}0$	6.31	4.24	—	5.14
$4\bar{7}3$	8.57	9.77	8.77	9.02	$2\bar{11}9$	2.19	1.42	1.82	1.77
$2\bar{7}5$	6.10	5.74	3.86	4.11	$6\bar{12}6$	2.63	1.16	—	1.83
$1\bar{7}6$	2.74	0.60	1.88	1.42	$5\bar{12}7$	2.52	1.70	2.30	2.25
$6\bar{7}1$	4.04	2.32	1.95	1.73	$4\bar{12}8$	2.19	1.99	—	2.83
$4\bar{8}4$	2.46	0.25	—	1.14	$9\bar{13}4$	2.69	1.72	2.23	2.12

Case 1: Only one phase $\varphi = 99°$.
Case 2: Mixture of major and minor orientations. The ratio is 0.74:0.26.
Case 3: Mixture of f.c.c. major and minor orientations. The ratio is 0.47:0.46:0.07.

3. Results and discussion

Fig. 1 shows a transmission electron micrograph of C_{60} thin film composed of many platelet crystals. The crystals are mostly truncated triangular or hexagonal in shape, in which the {111} lattice plane is parallel to the substrate surface. Fig. 2 shows a typical electron diffraction pattern of the crystal recorded on an IP with the {111} plane parallel to the substrate. This keeps a sixfold rotational symmetry corresponding to the $Pa\bar{3}$ space group. The existence of *hkl* ($h + k$, $k + l$, $l + h$: odd; *i.e.* forbidden reflections for f.c.c.) reflections and the nonexistence of mirror symmetry in the diffraction pattern are characteristic compared with the f.c.c. diffraction at room temperature. Table 1 shows 46 symmetrically independent intensities collected from 306 diffraction spots measured in <111> incidence with the diffraction image recorded on an IP. The lattice constant is 1.404 nm and the outer-most Bragg spot $(9, \bar{13}, 4)$ has a spacing of 0.086 nm.

Several workers have carried out the crystal structure analysis on C_{60} below the glass transition point (86 K) by X-ray and neutron scattering, where the fitting of the intensity profile was carried out using a rotational angle φ as a parameter for the model with space group $Pa\bar{3}$. Here φ denotes a rotation angle of the molecule at the origin of the unit cell around the [111] threefold inversion rotation axis from the initial setting, where the initial setting is defined as a setting with three mirror planes of the molecule normal to the three unit-cell axes (Heiney *et al.*, 1991; Sachidanandam & Harris, 1991; David *et al.*, 1991), see Fig. 3(*a*). At this setting, each mirror plane is parallel with the *ab*, *bc* or *ac* plane of the unit cell. The best fit was found at $\varphi \simeq 98°$. David (David, Ibberson & Matsuo, 1993) analyzed neutron scattering data below the first-order transition point (260 K) in detail and pointed out that there are two crystal modifications, which they called the major and the minor orientations. The major orientation is the setting at $\varphi \simeq 98°$ and the minor orientation is that with a rotation angle of $\varphi \simeq 38°$ (differing 60° from the major orientation). In the major orientation a pentagon in the molecule faces a 6:6 bond of the nearest neighboring molecule along [110]. On the other hand, in the minor orientation a hexagon faces a 6:6 bond of the nearest neighboring molecule. Accordingly, the major orientation is a somewhat favorable structure in interaction energy among the adjacent molecules owing to the fact that an electron-poor pentagon faces an electron-rich 6:6 bond in the major orientation (see Fig. 4). David and coworkers (David, Ibberson & Matsuo, 1993) suggested that these two configurations were interchangeable with each other through a simple rotational hopping around $[1\bar{1}0]$, $[01\bar{1}]$ or $[\bar{1}01]$ with an angle of 41.81° [= arcsin(2/3)], when above the glass transition point. Below the glass transition point the hopping is frozen. From their neutron scattering data, the ratio of the major and minor orientations was determined to be

~ 0.64 at 200 K, which is increased to ~ 0.84 at the glass transition temperature and becomes constant below that temperature.

In the following we discuss the least-squares fit of the observed scattering intensities from the thin C_{60} crystal at liquid helium temperature with those calculated kinematically from a model structure, where we used the lattice constant a = 1.404 nm for the cubic lattice, the 6:6 bond = 0.140 nm and the 6:5 bond = 0.145 nm. The least-squares fit was performed with the scaling factor and the temperature factor as parameters. At the first step we considered a model with rotation angle φ as a structural parameter, as in the above-mentioned X-ray and neutron experiments in order to confirm the applicability of the IP method to electron diffraction. Secondly, we considered the coexistence ratio of the major and the minor orientations. Fitting by scaling and temperature factors was performed for the various coexistence ratios. Finally, in addition to the major and the minor orientations, the f.c.c. component, which indicates a f.c.c. lattice structure with a freely rotating C_{60}, was introduced in order to refine the fitting.

The least-squares fit by the model with a rotation angle was carried out for every degree of the rotation angle. Fig. 5 shows the resultant R factor as a function of the φ values. The R factor reaches the minimum value of 0.23 at $\varphi \simeq 99°$ (Case 1 in Table 1), where the temperature factor is 0.0565 nm^2. Although the temperature factor seems large at liquid helium temperature, the factor used here can be attributed not only to a pure temperature factor, but also to the decrease of intensity with increasing excitation error at higher scattering angles due to a kind of Lorentz factor arising from the diffraction geometry characteristic of electron diffraction. The rotation angle $\varphi \simeq 99°$ coincides well with that of the major orientation (97.62°) already reported, which indicates that the C_{60} molecule in a thin film tends to exist in the major orientation at liquid helium temperature.

As the second step of analysis we tried to estimate the coexisting ratio between the major and minor orientations by the least-squares fitting of observed intensities as in the case of David and coworkers (David, Ibberson & Matsuo, 1993). For estimation we used the 33 reflections which are forbidden in $Fm\bar{3}$ of f.c.c.

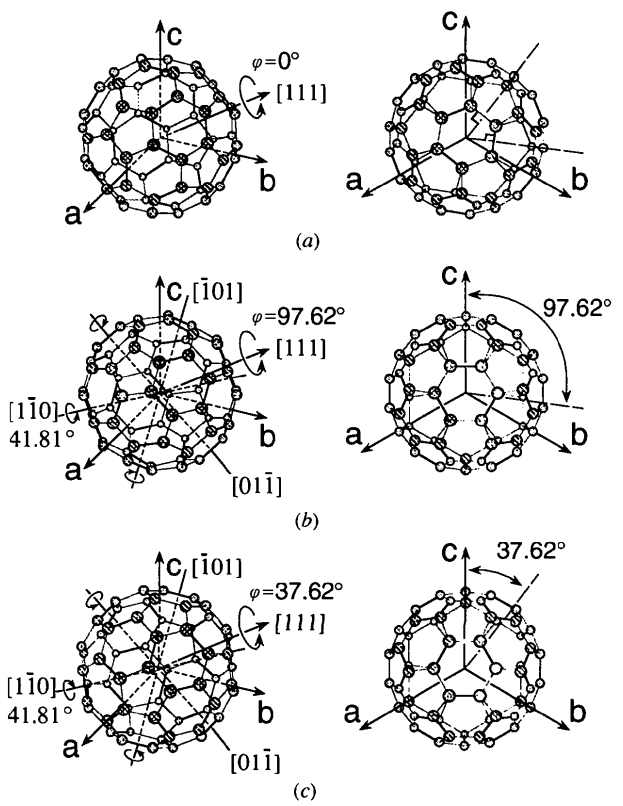

Fig. 3. Orientation of the molecule at the origin of the unit cell in the low-temperature phase of C_{60} (left) and their projections on (111) (right). (*a*) Initial setting, φ = 0°; (*b*) major orientation, φ = 97.62°; (*c*) minor orientation, φ = 37.62°.

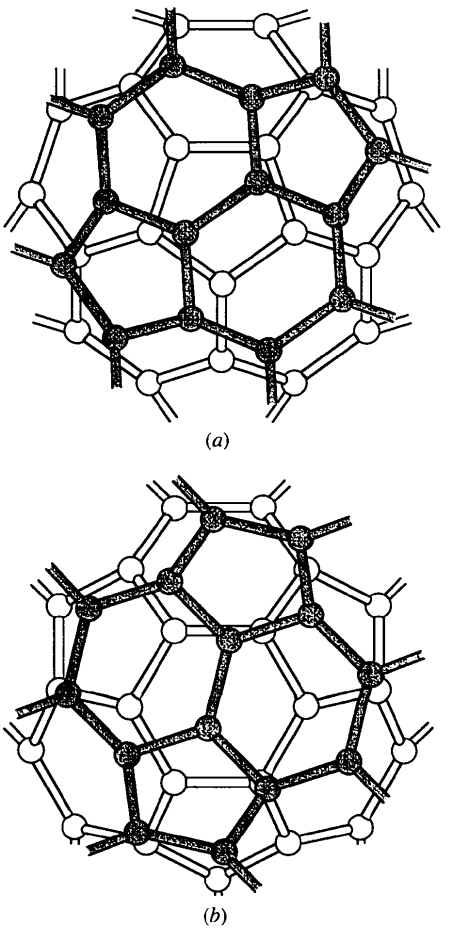

Fig. 4. Configurations of neighboring molecules projected along [110]. (*a*) Major orientation; (*b*) minor orientation.

crystals, but allowed in $Pa\bar{3}$. As discussed later, there is the possibility that the sample contains an additional disordered region of molecular orientation due to the rapid freezing of molecules at each random orientational angle, which means here an f.c.c. component. The intensities of forbidden reflections for f.c.c. should not be disturbed by the f.c.c. component and, therefore, the 33 reflections were used for the least-squares fitting. In the fitting we have to consider additional parameters: the ratios of [111] incidence and $[\bar{1}\bar{1}\bar{1}]$ incidence, because the scatterings at the [111] and $[\bar{1}\bar{1}\bar{1}]$ incidences were not the same but had mirror symmetry. This concept indicates that the C_{60} crystal is composed of many thin domains whose boundaries are the 111 plane. Fig. 6 shows the contour map of the R factor minimized by least-squares fitting of the observed and kinematically calculated intensities for each major:minor ratio and [111]:$[\bar{1}\bar{1}\bar{1}]$ ratio. It is assumed here that the latter ratios in the major and minor orientations are equal. The minimum R factor of 0.17 is obtained at major:minor = 0.74:0.26 and [111]:$[\bar{1}\bar{1}\bar{1}]$ = 0.87:0.13 and a temperature factor of 0.0314 nm^2. The ratio of the major and minor orientations, 0.74, is slightly different from the value of 0.84 obtained for the bulk by David and cowrokers (David, Ibberson & Matsuo, 1993). The R factor is decreased from 0.23 to 0.17 by assuming the coexistence of major and minor orientations (see case 2 in Table 1).

Since the R factor of 0.17 still seems unsatisfactory, an extra parameter to be minimized has to be considered. That is, the existence of the f.c.c. component in the sample was considered, so that the ratio among the major, minor and f.c.c. components was determined in the fitting procedure. In this case we took account of the ratio of [111] and $[\bar{1}\bar{1}\bar{1}]$ incidences separately for each orientation. Fig. 7 shows the R factor of the best fit, where the minimum value of the R factor (0.12) is obtained at the f.c.c.:major:minor ratio 0.47:0.46:0.07, with [111]:$[\bar{1}\bar{1}\bar{1}]$ = 0.88:0.12 for the major orientation and [111]:$[\bar{1}\bar{1}\bar{1}]$ = 1.00:0.00 for the minor orientation. The temperature factor is 0.0354 nm^2. A reason for the large fraction of the f.c.c. component might be that the sample was instantaneously cooled down to $\sim$ 90 K from room temperature in a specimen exchange chamber of cryo-TEM and then transferred into the specimen stage of TEM kept at 4.2 K, so that the cooling rate was too fast for sufficient ordering of the molecular orientation.

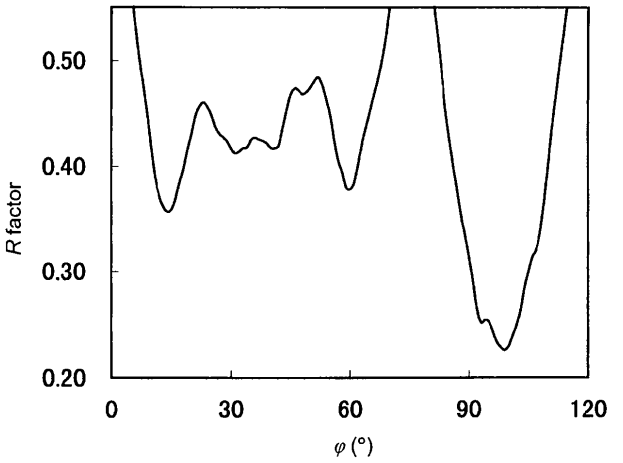

Fig. 5. R factor against the rotation angle φ. The observed intensities were fitted with kinematically calculated values at each φ by least-squares for the scaling factor and the temperature factor as parameters. The minimum R factor was attained for $\varphi \simeq 99°$, corresponding to the major orientation. The temperature factor was 0.0565 nm^2.

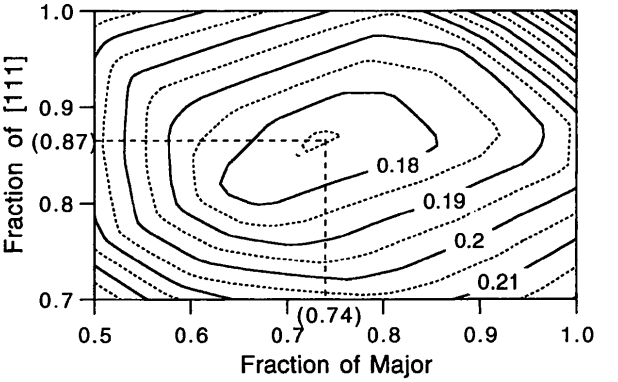

Fig. 6. Contour map of the R factor calculated for each major:minor ratio and [111]:$[\bar{1}\bar{1}\bar{1}]$ ratio using the scaling and temperature factors determined by the least-squares fit of the observed and kinematically calculated intensities.

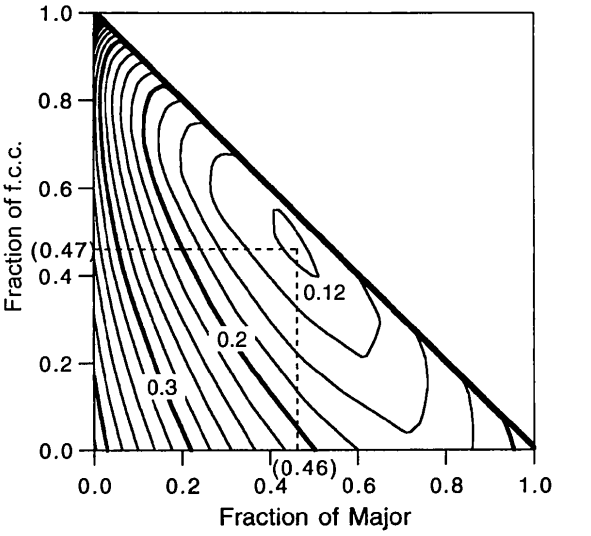

Fig. 7. Contour map of the R factor calculated for each major, minor and f.c.c. fraction, where the scaling and temperature factors are determined by the least-squares fit of the observed and kinematically calculated intensities. The [111]:$[\bar{1}\bar{1}\bar{1}]$ ratio was also a fitting parameter in the fitting procedure and this figure is the best result with [111]:$[\bar{1}\bar{1}\bar{1}]$ = 0.88:0.12 for the major and 1.00:0.00 for the minor orientations.

As a result, some molecules are expected to transform into a glassy state without passing through the low-temperature phase. The major:minor ratio of 0.46:0.07 (= 0.87:0.13) corresponds well to the results of the neutron scattering experiment by David and coworkers (David, Ibberson & Matsuo, 1993). The R factor is reduced to 0.12, considering the existence of some fraction of f.c.c. (Case 3 in Table 1).

In the above calculations kinematical scattering intensities were used as the calculated intensities fitting with the observed ones. Here the dynamical effect is estimated to confirm the validity of kinematical calculation in the present case. The dynamical scattering amplitudes were calculated by the multi-slice method. The dynamical scattering amplitudes were calculated only for an ideal crystal having the major orientation. Fig. 8 shows the calculated dynamical scattering patterns of major orientation for [111] incidence. The reflection spots are normalized by the strongest reflection $2\bar{2}0$ and plotted up to reflections with intensities three orders lower than the $2\bar{2}0$. By increasing the crystal thickness [from (*a*) to (*e*) in the figure], the whole intensity profile in the diffraction pattern becomes monotonous as a function of the scattering angle. The observed pattern shown in (*f*) resembles that calculated with 5 or 10 nm crystal thickness (*a*) or (*b*). We carried out the fitting of the observed intensities with the calculated dynamical scattering intensities. Fig. 9 represents the R factor determined by comparing the calculated intensities with the dynamical scattering for each crystal thickness. The R factor is minimized to a value of 0.22 at ~ 6 nm, which agrees well with the visual comparison of the diffraction pattern shown in Fig. 8. Fig. 10 shows the calculated dynamical scattering amplitudes of several representative reflections of the major orientation. For most reflections, except some weak reflections in the high-angle region, the linearity between the scattering amplitude and crystal thickness was held at 10 nm or more and, therefore, the kinematical treatment of the scattering seems appropriate in the present case. The R factor in Fig. 9, in fact, is almost constant within 1% variation up to ~ 10 nm, which shows that scattering from a crystal in this thickness range may be treated kinematically.

In this sample it is shown from the above estimation that the specimen used in this work is thin enough and contains no heavy atoms. Therefore, the dynamical scattering effect is negligible, as described above. However, the R factor does not fall lower than 0.23 when an attempt was made to fit the observed intensities only with those calculated based on one structural component structure, *i.e.* the major orientation. By assuming the coexistence of a minor orientation crystal and also a f.c.c. crystal with the random molecular orientation, the R factor could be reduced to 0.17 and 0.12, respectively. The minor orientation and random orientation of f.c.c. structures are regarded as disordered structures in the major orientation crystal. Thus, the structural disorder in a specimen may be one key factor to be considered in structure analysis by electron crystallography. Compared with X-ray or neutron scattering experiments, the specimens for electron microscopy are so small or so thin that the disordered structure works more effectively in diffraction, which results in a higher R factor. Of

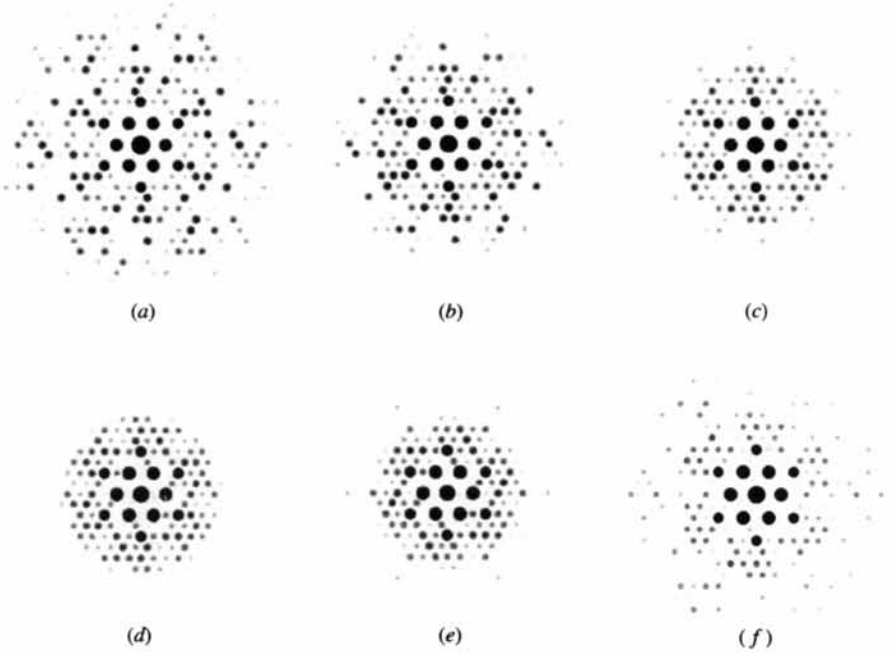

Fig. 8. Calculated dynamical diffraction patterns of the major orientation crystal for <111> incidence using the multi-slice method for several crystal thicknesses [λ = 0.00164 nm for 400 kV, Δz = 0.608 nm for (111) lattice spacing]: (*a*) 5, (*b*) 10, (*c*) 15, (*d*) 20, (*e*) 25 nm and (*f*) schematic drawing of the observed diffraction pattern. All the intensities are scaled by that of each $2\bar{2}0$ reflection and illustrated up to the spots with three orders lower intensity than that of the $2\bar{2}0$ reflection so as to be compared with the observed pattern.

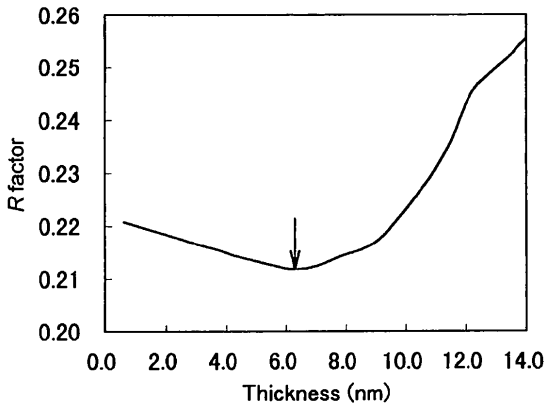

Fig. 9. *R* factor derived from the scaling factor and temperature factor determined by the least-squares fit of the observed and dynamically calculated intensities for the major orientation crystal with the incident beam of <111> for each crystal thickness.

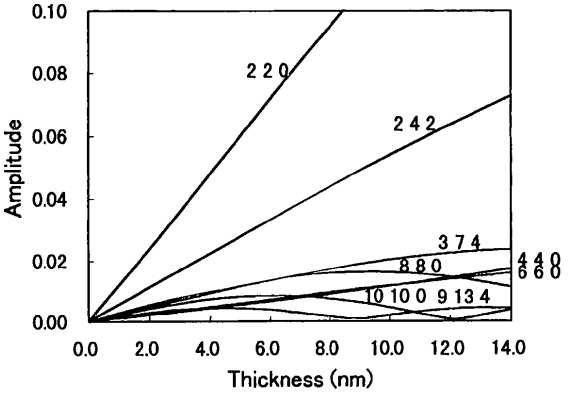

Fig. 10. Dynamical scattering amplitudes of the major orientation crystal calculated by a multi-slice method. Although the outermost (9, 13, 4) reflection shows deviation from kinematical scattering, the intensity is too small to make a considerable contribution to the fitting with the observed intensities at the *R* factor range 0.1–0.2.

course, the dynamical effect surely exists as shown by the higher angle reflections in Figs. 8 and 10, and must be considered in the analysis procedures to reduce the *R* factor to a reliable value below 0.10.

References

David, W. I. F., Ibberson, R. M., Dennis, T. J. S., Hare, J. P. & Prassides, K. (1992). *Europhys. Lett.* **18**, 219–225.

David, W. I. F., Ibberson, R. M. & Matsuo, T. (1993). *Proc. R. Soc. London Ser. A*, **442**, 129–146.

David, W. I. F., Ibberson, R. M., Matthewman, J. C., Prassides, K., Dennis, T. J. S., Hare, J. P., Kroto, H. W., Taylor, R. & Walton, D. R. M. (1991). *Nature*, **353**, 147–149.

Dorset, D. L. (1991). *Ultramicroscopy*, **38**, 23–40.

Dorset, D. L. (1995). *Structural Electron Crystallography*. New York, London: Plenum Press.

Heiney, P. A., Fischer, J. E., McGhie, A. R., Romanow, W. J., Denenstein, A. M., McCauley Jr, J. P., Smith III, A. B. & Cox, D. E. (1991). *Phys. Rev. Lett.* **66**, 2911–2914.

Ishiguro, T. & Hirotsu, Y. (1992). *Jpn. J. Appl. Phys.* **31**, L481–483.

Isoda, S., Saitoh, K., Moriguchi, S. & Kobayashi, T. (1991). *Ultramicroscopy*, **35**, 329–338.

Johnson, R. D., Meijer, G. & Bethune, D. S. (1990). *J. Am. Chem. Soc.* **112**, 8983–8984.

Kroto, H. W., Heath, J. R., O'Brien, S. C., Curl, R. F. & Smalley, R. E. (1985). *Nature*, **328**, 162–163.

Matsuo, T., Suga, H., David, W. I. F., Ibberson, R. M., Fabre, C., Rassat, A. & Dworkin, A. (1992). *Solid State Commun.* **83**, 711–715.

Ogawa, T., Moriguchi, S., Isoda, S. & Kobayashi, T. (1994*a*). *Polymer*, **35**, 1132–1136.

Ogawa, T., Moriguchi, S., Isoda, S. & Kobayashi, T. (1994*b*). Proceedings of the Thirteenth International Congress on Electron Microscopy, Vol. 1, pp. 965–966. Les Ulis: Les Editions de Physique.

Sachidanandam, R. & Harris, A. B. (1991). *Phys. Rev. Lett.* **67**, 1467.

Yannoni, C. S., Bernier, P. P., Bethune, D. S., Meijer, G. & Salem, J. R. (1991). *J. Am. Chem. Soc.* **113**, 3190–3192.